Theoretical investigation of band-gap and mode characteristics of anti-resonance guiding photonic crystal fibres*

Yuan Jin-Hui(苑金辉)[a)†], Sang Xin-Zhu(桑新柱)[a)], Yu Chong-Xiu(余重秀)[a)], Xin Xiang-Jun(忻向军)[a)], Zhang Jin-Long(张锦龙)[a)], Zhou Gui-Yao(周桂耀)[b)], Li Shu-Guang(李曙光)[b)], and Hou Lan-Tian(侯蓝田)[b)]

[a)] *Key Laboratory of Information Photonics and Optical Communications (BUPT), Ministry of Education; Institute of Optical Communication and Optoelectronics, Beijing University of Posts and Telecommunications, Beijing* 100876, *China*

[b)] *Institute of Infrared Optical Fibres and Sensors, College of Information Science and Engineering, Yanshan University, Qinhuangdao* 066004, *China*

(Received 21 March 2010; revised manuscript received 20 August 2010)

With the full-vector plane-wave method (FVPWM) and the full-vector beam propagation method (FVBPM), the dependences of the band-gap and mode characteristics on material index and cladding structure parameter in anti-resonance guiding photonic crystal fibres (ARGPCFs) are sufficiently analysed. An ARGPCF operating in the near-infrared wavelength is shown. The influences of the high index cylinders, glass interstitial apexes and silica structure on the characteristics of band-gaps and modes are deeply investigated. The equivalent planar waveguide theory is used for analysing such an ARGPCF filled by the isotropic materials, and the resonance and the anti-resonance characteristics can be well predicted.

Keywords: anti-resonance guiding photonic crystal fibres, full-vector plane-wave method, full-vector beam propagation method, band-gap and mode characteristics

PACS: 42.70.Qs, 42.81.–i, 71.15.Ap **DOI:** 10.1088/1674-1056/20/2/024213

1. Introduction

Because of the air holes distributed along the longitudinal direction in the cladding region, the light energy is confined mainly in the solid core region by total internal reflection at the interface between the silica core and holey cladding. Hollow-core photonic crystal fibres[1−8] (HC-PCFs) guide light through Bragg scattering effect,[9] and the band-gaps are formed by resonance effects of different cladding structures. Anti-resonance guiding photonic crystal fibres[10−12] (ARGPCFs) with a periodic array of high index cylinders in the cladding cannot guide light by total internal reflection due to the inverted index contrast.[13] With the model of anti-resonance guiding reflecting-optical waveguide (ARROW), proposed by Yariv and Marom,[9] Litchinister *et al.*[14] theoretically investigated the transmission characteristics of ARROW, where they established a simple model and predicted the band-gap and mode properties. Birks *et al.*[15] analysed the formation mechanism of band-gaps in ARROW with an approximate method, and they showed that the confinement of high index cylinders on the light energy was similar to the scattering effect of single plane waveguide. In previous reports,[14,15] Litchinister and Birks *et al.* considered primarily the influence of single high index cylinders on the characteristics of band-gaps and modes. Recently, Couny *et al.*[16] described the existing characteristics of Bloch modes, and showed three kinds of resonances for band-gap formation in cladding structures including the glass interstitial apexes, the silica structure for joining the neighbouring apexes and air holes.

*Project partly supported by the National Key Basic Research Special Foundation of China (Grant Nos. 2010CB327605 and 2010CB328300), the National High-Technology Research and Development Program of China (Grant No. 2009AA01Z220), the Key Grant of the Chinese Ministry of Education (Grant No. 109015), the Discipline Co-construction Project of Beijing Municipal Commission of Education, China (Grant No. YB20081001301), the Open Fund of Key Laboratory of Information Photonics and Optical Communications (Beijing University of Posts and Telecommunications), Chinese Ministry of Education, and the Specialized Research Fund for the Doctoral Program of Beijing University of Posts and Telecommunications (Grant No. CX201023).

†Corresponding author. E-mail: yuanjinhui81@163.com

© 2011 Chinese Physical Society and IOP Publishing Ltd

Here, the dependences of the band-gap and the mode characteristics on the material index and structure parameter in ARGPCF are sufficiently analysed. Based on a designed ARGPCF, the influences of high index cylinder, glass interstitial apex and silica structure on the characteristics of band-gap and mode are deeply investigated. The equivalent planar waveguide theory can be used for well predicting the resonance and the anti-resonance characteristics of such an ARGPCF filled by the isotropic materials.

2. Band-gap and mode characteristics

The cross section of photonic crystal fibre (PCF) is shown in Fig. 1(a). Insert of Fig. 1(a) shows the triangle arrange lattice where the hole diameter d, pitch Λ, glass interstitial apex and the silica structure are labeled. Figure 1(b) shows the three-dimensional propagation field of Gauss-like pulse, and the insert corresponds to the transverse field distribution of fundamental mode, which shows that a doublet of degenerate mode reaches its maximum at the centre of the fibre core and monotonically decreases with the distance from the fibre centre. The parameters are as follows: $d = 1.5$ μm, $\Lambda = 2.5$ μm, air filling fraction $f = 0.6$, and the silica and air indices are 1.45 and 1.0 respectively.

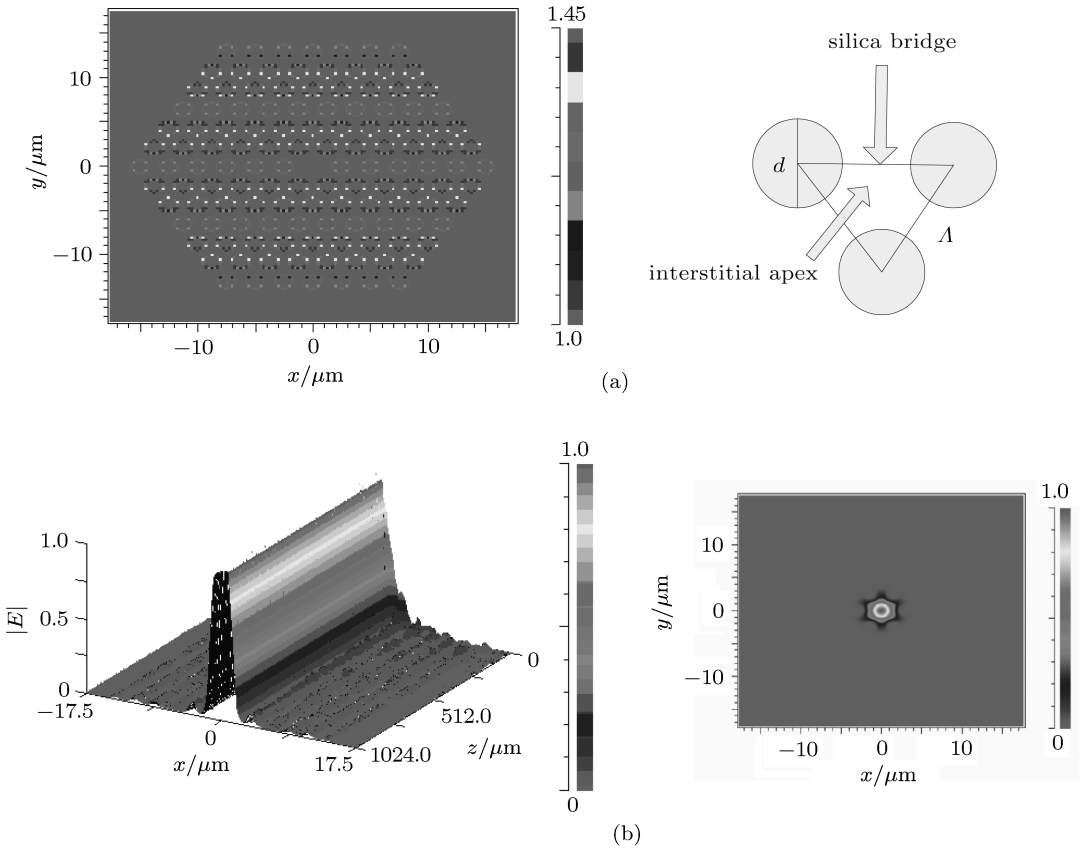


Fig. 1. (a) Cross section of solid core PCF, and (b) propagation field of Gauss-like pulse. Inserts on the right-hand sides of panels (a) and (b) show the triangle arrange unit and transverse field distribution of fundamental mode respectively.

2.1. Dependences of band-gap and mode on material index

The ARGPCFs can be obtained by filling higher index materials into the cladding holes. The plots for normalized frequency $k\Lambda$ as a function of normalized propagation constant $\beta\Lambda$ with different filled materials are presented in Fig. 2 with the full-vector plane-wave method (FVPWM).[17,18]

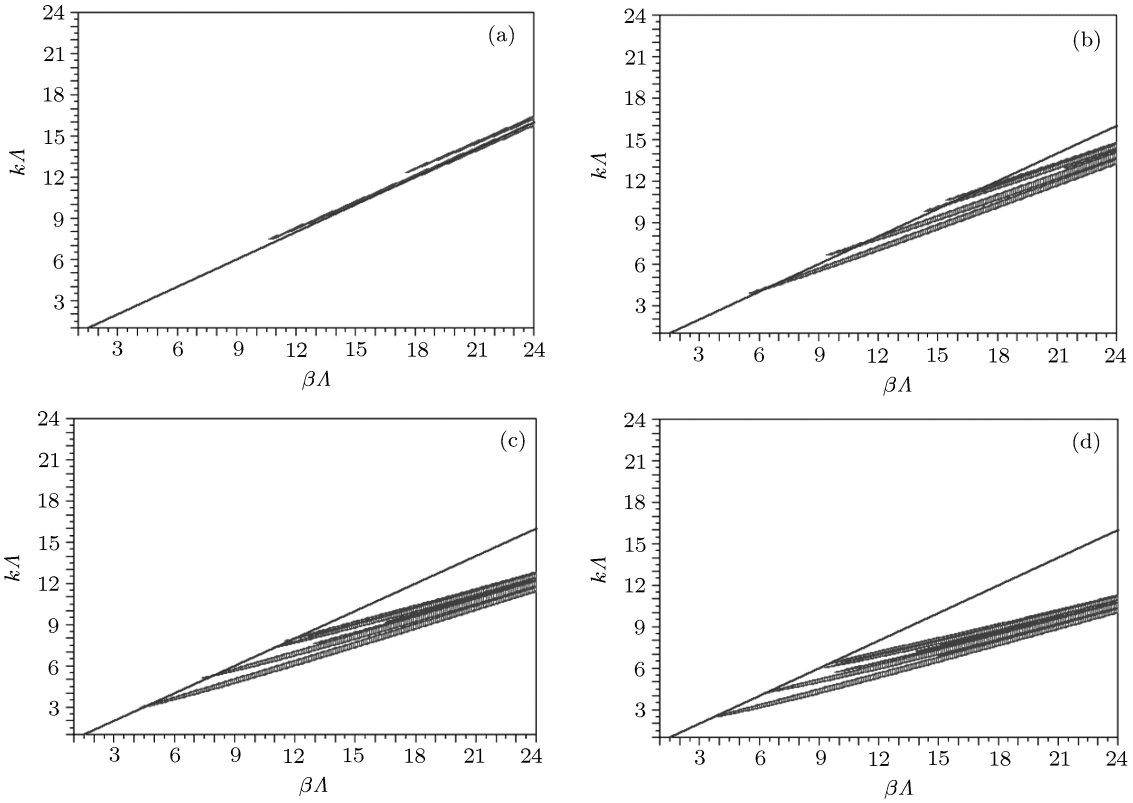


Fig. 2. Plots for normalized frequency $k\Lambda$ as a function of normalized propagation constant $\beta\Lambda$ with material indices are (a) 1.5, (b) 1.7, (c) 1.9 and (d) 2.1.

According to the optical waveguide theory, the effective refractive index of guided-mode $n_{\text{eff}} = \beta/k$ should satisfy $n_2 < n_{\text{eff}} < n_1$, where n_1 and n_2 are respectively the indices of silica material and space filling fundamental mode, determined by the complex topology structure of cladding region and the higher index material filled. The out-plane band-gaps (above silica line, as shown in Fig. 2) are primarily considered. In Fig. 2(a), when the material index is 1.5, the band-gap district in a $k\Lambda$ range from 8 to 16 corresponds to that in a $\beta\Lambda$ range from 10.5 to 24. The material index is chosen as 1.7 in Fig.2 (b), the band-gaps intersect with the silica line, and the positions of band-gaps distinctly shift toward longer wavelengths with $\beta\Lambda$ increasing from 5.6 to 19 and $k\Lambda$ increasing from 4 to 12. As shown in Figs. 2(c) and 2(d) with material indices 1.9 and 2.1 respectively, the positions of band-gaps shift toward below the silica line, and the input light energy will entirely leak into the cladding structures. Moreover, the band-gap district becomes narrower as the $k\Lambda$ increases, and the mode numbers in band-gap will gradually decrease and shrink to a series of degenerate states. With the full-vector beam propagation method (FVBPM),[19] the transverse field distributions of propagation modes corresponding to Figs. 2(a)–2(d) are shown in Fig. 3.

In Fig. 3(a), the light energy is distributed all over the cross section, and reaches up to 40% of the total energy in the core region. The intensity ratio between the high index cylinders and silica structure is about 2:1 in the cladding region, indicating the integrated influence of three kinds of resonances on band-gap transmission. In the weakly-guided approximation in Fig. 3(a), the Bloch-modes exist in the cladding region, and it agrees well with the experimental observation of the cladding Bloch-modes in the near-field and Fresnel-zone.[16]. In Figs. 3(b)–3(d), as the material index increases from 1.7 to 2.1, the light energy is primarily confined in the high index cylinders, and the energy intensity in the core region gradually decreases. When the material index reaches up to 1.9 and 2.1, the energy is distributed only in the inner several rings, and no energy is observed in the core region. The high index cylinders as plane optical waveguide plays a primary role due to enhanced index contrast between the cladding and core region, at some time the influences of glass interstitial apex and silica structure can be neglected.

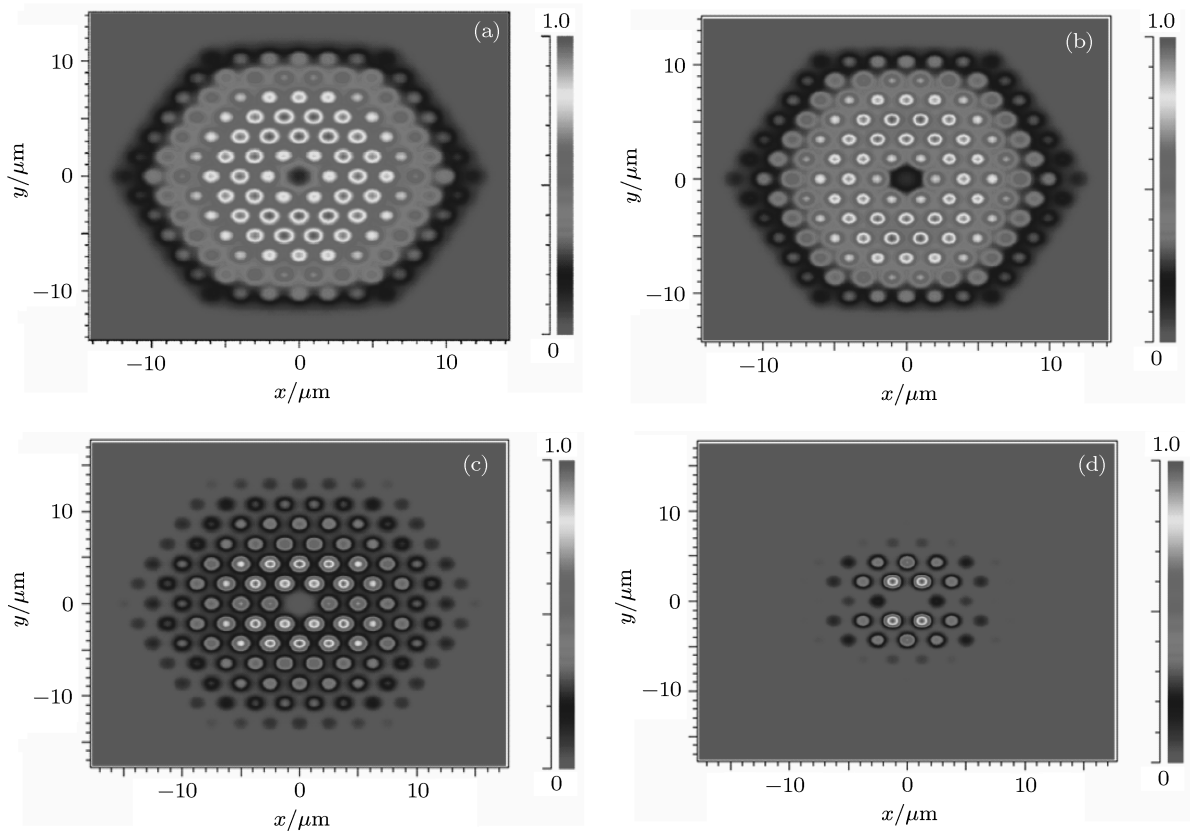


Fig. 3. Transverse field distributions of propagation modes over 1-mm distance.

2.2. Influences of structure parameter on band-gap

The structure parameters are crucial for the light energy propagating in the band-gaps. The relations between relative position ($1/\lambda$) and hole diameter (d), between relative position ($1/\lambda$) and pitch (Λ), and between relative position ($1/\lambda$) and material filling fraction (f) are presented in Figs. 4(a), 4(c) and 4(d) respectively.

As shown in Fig. 4(a), the positions of band-gaps shift from 1.98 μm to 2.22 μm as d increases from 0.5 μm to 4 μm, and the slope is nearly a constant of -0.45. The high index cylinders become much closer to each other with a larger d value, and the photonic crystal cladding appears like a two-dimensional waveguide structure, which can be treated as a homogeneous material at longer wavelengths. The light energy will be distributed all over the high index cylinders, glass interstitial apexes and silica structures. In Fig. 4(b), the up-boundaries of band-gaps shift from 0.6 to 0.52 with Λ increasing from 3 μm to 5.5 μm, but the down-boundaries keep nearly invariable. The positions and widths of band-gaps take on lesser fluctuation after 5.5 μm. The primary reason is considered as follows: when Λ increases to a certain value and $\lambda/\Lambda \ll 1$, the high index cylinders appear more like an array of individual waveguide, and the light energy is primarily confined into the cylinders. Thus, it shows insensitive to Λ. The relation between the relative positions of band-gap and f is shown in Fig. 4(c). The positions of band-gap change from 2 μm to 2.247 μm in the f range of 0.1 to 1.0, and the corresponding slope efficiencies are about -55% and -40% with f changing from 0.1 to 0.4 and 0.4 to 1.0 respectively. The changing trend is similar to that in Fig. 4(a) except that the bending direction of up-boundary is contrary (curvature > 0 in Fig. 4(a) and curvature < 0 in Fig. 4(c)). The contrary curvature arises from the wave-vector inverse induced by fluctuations of structure parameters, and it will give rise to variation of boundary condition of electromagnetic field when the plane waves are expanded in the first Brillouin zone. When f reaches up to 1.0, it can be equivalent to the step-index profile. The characteristics of band-gaps completely depend on the complex properties of higher index material such as absorbing and scattering.

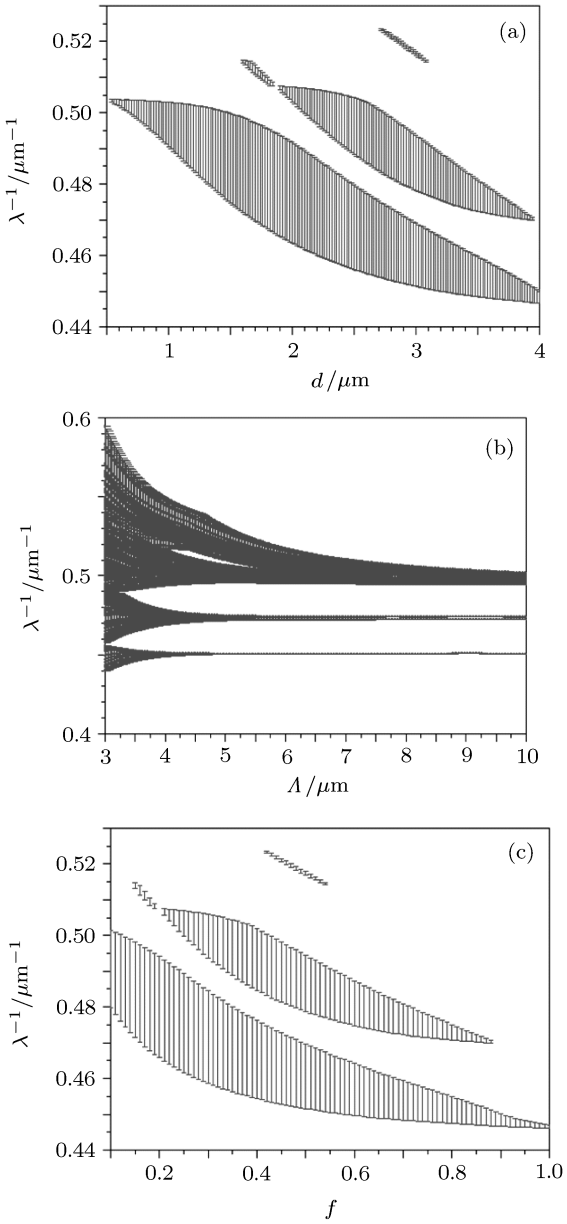


Fig. 4. Relative positions versus (a) hole diameter of band-gap d, (b) pitch Λ, and (c) material filling fraction f.

3. Design of ARGPCF in near-infrared wavelength

Based on the above analysis, an ARGPCF in near-infrared wavelength is designed. The ARGPCF with background silica and filled material indices of 1.45 and 1.6 has the same cladding structure as that shown in Fig. 1(a). The structure parameters are $d = 1.2$ μm, $\Lambda = 2.0$ μm, and core diameter $D = 5.3$ μm. As depicted in Fig. 5(a), the material index is distributed symmetrically along the transverse direction and the longitudinal direction. The corresponding part of transverse dielectric constant profile at $z = 0$ is shown in Fig. 5(b).

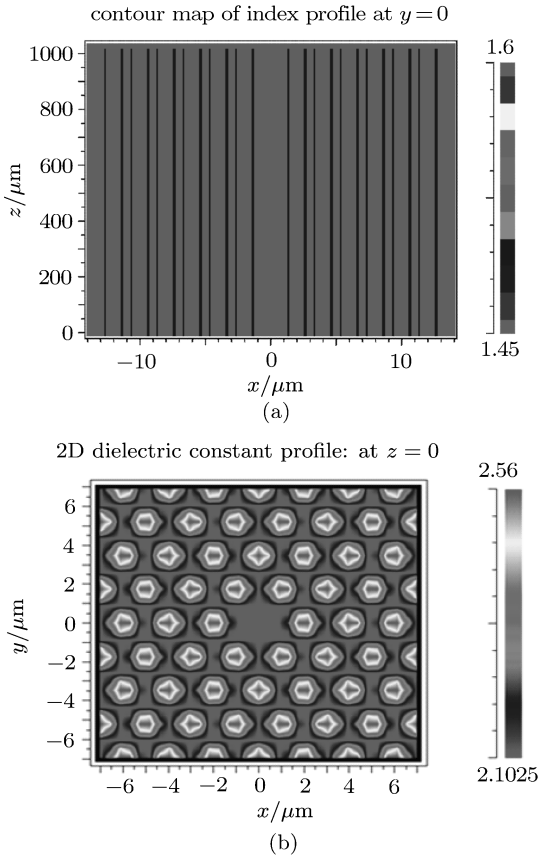


Fig. 5. (a) Distribution of material index along longitudinal direction, and (b) part of transverse dielectric constant profile at $z = 0$.

3.1. Band-gap characteristics

The propagation diagram for such an ARGPCF is shown in Fig. 6. Insert corresponds to the symmetry point configuration in the first Brillouin zone.

Figure 6 shows the out-plane band-gaps with $k\Lambda$ changing from 5.5 to 17, which corresponds to the wavelength range of 0.74 μm to 2.485 μm. As the normalized wave-vector $k\Lambda$ decreases, the upper allowed-bands (below silica line) will shrink to an extremely narrow region, and the light energy is well localized within high index cylinders. On the contrary, the light energy will diffuse into the glass interstitial apexes and silica structure. Insert (on the right-hand side) shows the symmetric points Γ, M, and K in first Brillouin zone, which play different roles in band-gaps formation. At the Γ-point of the reciprocal lattice Brillouin zone, the modes below silica line may be symmetric or anti-symmetric. The symmetric form is characterized by the fields in all cylinders being in-phase with one another, whereas the field changes sign between the

nearest neighbour apexes for anti-symmetric modes. The symmetric modes are the fundamental space filling mode and form the upper boundary in-plane band-gaps (below silica line). Correspondingly, the anti-symmetric modes form the upper boundary of out-plane band-gaps (above silica line), and the high index cylinders are considered as the most important optical resonators associated with the upper band-gaps edge. The lower edges of band-gaps are formed from the trajectories of two cladding modes with different symmetries in apexes and silica structure, corresponding to K-point and M-point within the Brillouin zone. Comparing with HC–PCF, there exist no structures for connecting the high index cylinders in ARGPCFs. Most of light energy are confined in high index cylinders, and the anti-crossing events of guided-modes with glass features decrease.[20,21]

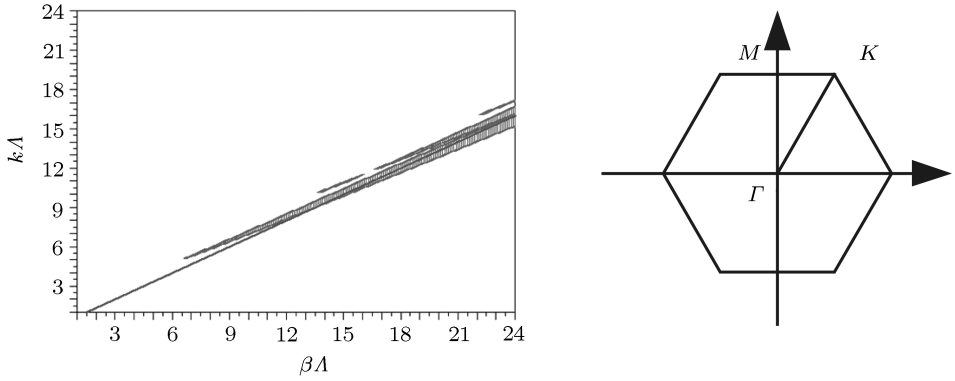
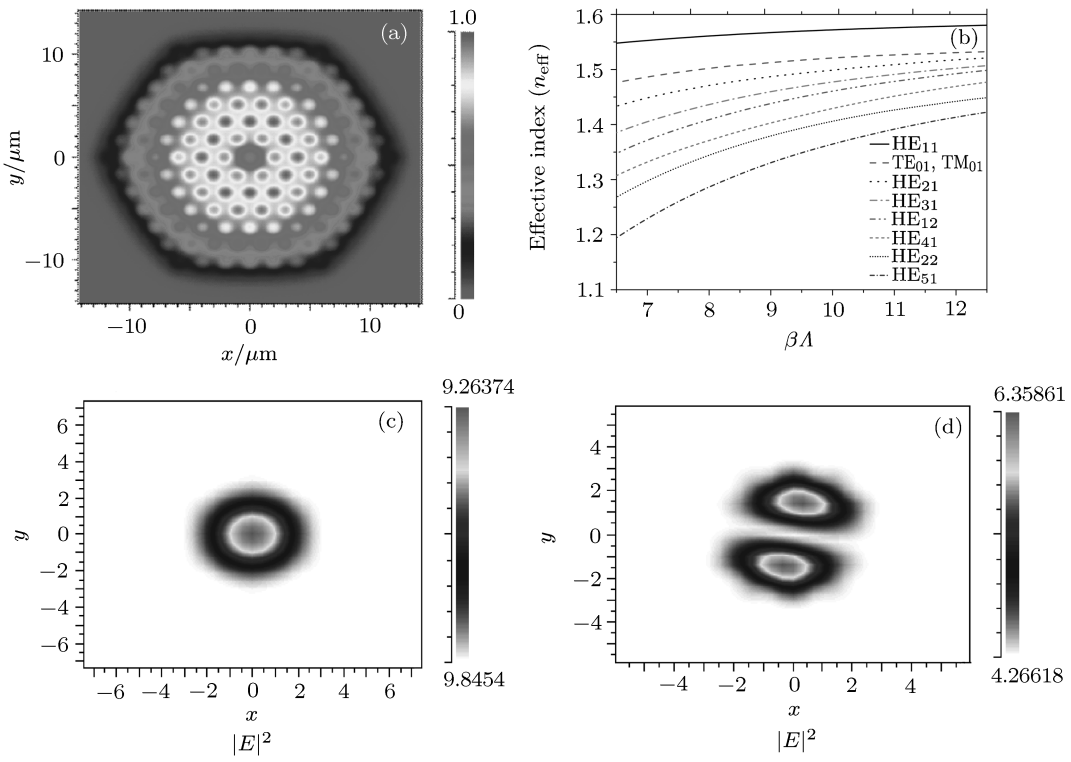


Fig. 6. Normalized wave-vector $k\Lambda$ as a function of normalized propagation constant $\beta\Lambda$. Insert (on the right-hand side) shows the first Brillouin zone symmetry point configuration.

3.2. Mode characteristics

Assuming that the light pulses of Gauss-like shape are launched into the core region at $z = 0$, the transverse field distributions and the existing mode forms of part of band-gap in high index cylinders over 1-mm distance are shown in Fig. 7.



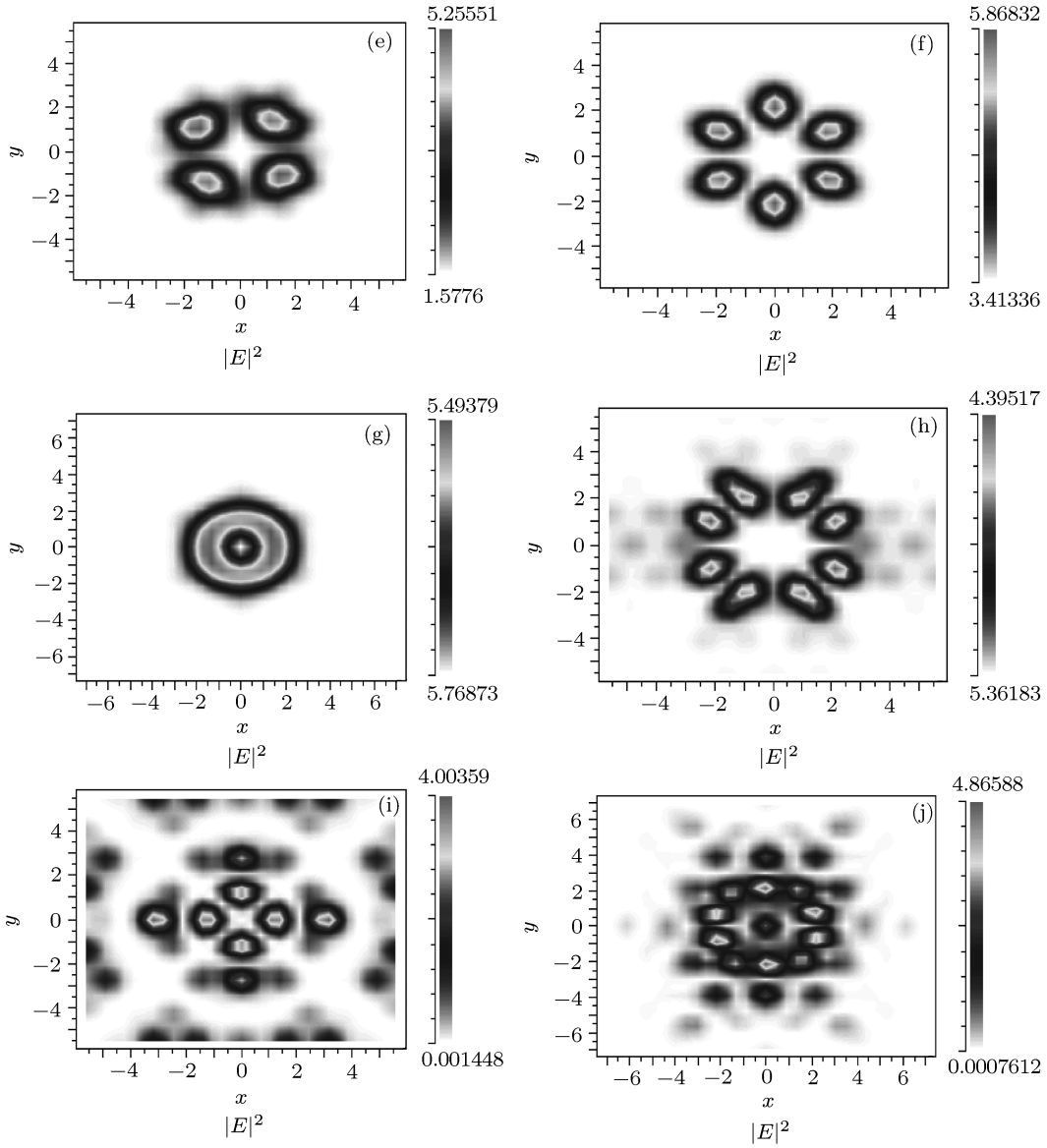


Fig. 7. (a) Transverse mode field distribution over 1 mm; (b) effective indices of modes in higher index cylinders as functions of normalized propagation constant $\beta\Lambda$; and figures (c), (d), (e), (f), (g), (h), (i) and (j) show the existing forms of HE_{11}, $TE_{01}(TM_{01})$, HE_{21}, HE_{31}, HE_{12}, HE_{41}, HE_{22}, and HE_{51} modes, respectively.

In Fig. 7(a), 40% and 60% mode field energies are distributed in the core and the cladding region respectively. The properties of light confined in the core region are introduced within an arrangement of cladding structures including the high index cylinders, glass interstitial apexes, silica structure. In particular, a strong confinement is related to the Fano resonance effect[22] caused by the interferences of different multi-pole components in the scattered field. Birks *et al.*[15] took into account the electromagnetic coupling between high index cylinders in the cladding region, and provided information about the width of cladding pass-bands. Sun *et al.*[23] analysed the transmission dips in the transmission spectrum which were determined by the resonance of an individual high index cylinder and coincided with the mode cut-offs in the cylinders. Considering the complex cut-off characteristics of modes, the anti-resonance effect and the resonance effect of different order modes in cladding structures correspond to the high transmission window and the high loss dip respectively. Figure 7(b) shows the plots for the effective index versus normalized propagation constant $\beta\Lambda$ for different order modes, i.e. HE_{11}, TE_{01} (TM_{01}), HE_{21}, HE_{31}, HE_{12}, HE_{41}, HE_{22}, and HE_{51} modes in the high index cylinders, and the effective index range from 1.1 to 1.6 with $\beta\Lambda$ changing from 6.5 to 12.5 is mainly considered. The anti-resonances and resonances between different

order modes in cladding structures emerge because of the more dispersive modes of high index cylinders intersecting with the modes in low index region. These resonance frequencies correspond to the transmission dips induced by the phase and loss matching between modes in different regions. For the lower-order mode such as HE_{11}, TE_{01} and TM_{01} modes which are well confined in the high index cylinders, the increases of effective indices are quite slow, and the relevant transmission dips are relatively broad. For HE_{21}, HE_{31}, HE_{12}, HE_{41}, HE_{22} and HE_{51} modes, the changes of effective indices are noticeable. Only narrow wavelength ranges need to leap from transmission dips to transmission windows. Moreover, these stopbands depend on the cut-off characteristics of modes in the whole cladding structures.[24,25] Figures 7(c), 7(d), 7(e), 7(f), 7(g), 7(h), 7(i) and 7(j) show the existing forms of HE_{11}, TE_{01} (TM_{01}), HE_{21}, HE_{31}, HE_{12}, HE_{41}, HE_{22}, and HE_{51} modes with the effective index $n_{\rm eff}$ values of 1.5812, 1.5335, 1.5265, 1.4925, 1.4855, 1.4635, 1.4385, and 1.4265 at $\beta\Lambda = 12$, respectively. These modes show discrepant characteristics of split cut-off at appointed $\beta\Lambda$. The HE_{11} mode shows a Gauss-like shape and the higher order modes show diverse symmetrical forms, existing in different polarization and degeneracy states. As seen from Fig. 7(b), the discrepancies of $n_{\rm eff}$ between different order modes are remarkable at lower $\beta\Lambda$, and the higher order modes especially HE_{41}, HE_{22}, and HE_{51} modes ($n_{\rm eff} < 1.45$) propagate mainly in the silica core. However, the discrepancies become less as $\beta\Lambda$ increases, and all modes will be confined in the high index cylinders. The band-gap districts diminish gradually, and the mode numbers will shrink to a series of degenerate states.

4. Discussion

The optical characteristics of the filled materials can be anisotropic or isotropic. For the anisotropic materials, the characteristics of band-gaps and modes are polarization-dependent, because the band-gap splitting and the polarization behaviour of the photonic state are induced by strong anisotropy of materials. Here only the isotropic materials are considered. For the isotropic materials, the polarization-dependent characteristics of band-gaps and modes can be neglected, and the multiple reflections from the high index materials and silica interfaces are used to analyse the mechanism of band-gap formation and visualize the propagation characteristics of modes. The transmission band frequencies are determined primarily by the geometries and the properties of the high index cylinders, and the high index cylinders can be equivalent to a series of planar waveguides.

The model of ARGPCF is considered as shown in Fig. 5(a). The periodic transmission tips and windows are determined by the characteristics of resonance and anti-resonance between modes in the low index core cylinders and the high index cylinders, which come into forming the phase and loss matching of modes. The mode characteristics of such an ARGPCF mainly depend on the mode structure in high index cylinders. The eigenmode equations for HE_{mn}, TE_{0n}, and TM_{0n} modes are described as

$$\frac{\mathrm{J}_{m-1}(U)}{U\mathrm{J}_m(U)} - \frac{\mathrm{K}_{m-1}(W)}{W\mathrm{K}_m(W)} = 0, \tag{1}$$

$$\frac{\mathrm{J}_1(U)}{U\mathrm{J}_0(U)} + \frac{\mathrm{K}_1(W)}{W\mathrm{K}_0(W)} = 0, \tag{2}$$

$$\frac{n_1^2\mathrm{J}_1(U)}{U\mathrm{J}_0(U)} + \frac{n_2^2\,\mathrm{K}_1(W)}{W\mathrm{K}_0(W)} = 0, \tag{3}$$

where $U^2 = (k_h^2 - k_{hz}^2)(d/2)^2$, $W^2 = (k_{hz}^2 - k_l^2)(d/2)^2$, $U^2 + W^2 = (k_h^2 - k_l^2)(d/2)^2$, k_h and k_l are the wavevectors in the high-index cylinders and silica structures, k_{hz} is the longitudinal component of k_h, while J_0, J_1, J_{m-1}, J_m and K_0, K_1, K_{m-1}, K_m correspond to the Bessel and transformative Bessel functions of 0, 1, $m-1$, and m orders, respectively.

The corresponding cut-off equation is given as

$$\mathrm{J}_m\left(k_{hx}\frac{d}{2}\right) = 0, \quad m \geq 0. \tag{4}$$

Here, k_{hx} corresponds to the transverse term of k_h. When $k_{hx}d/2 \gg m$, the cosine approximation leads to

$$\mathrm{J}_m\left(k_{hx}\frac{d}{2}\right) \approx \sqrt{\frac{2}{\pi k_{hx}\frac{d}{2}}}\cos\left(k_{hx}\frac{d}{2} - \frac{m\pi}{2} - \frac{\pi}{4}\right),$$

$$k_{hx}\frac{d}{2} - \frac{m\pi}{2} - \frac{\pi}{4} = \frac{(2l-1)\pi}{2}, \quad l = 0, 1, 2, \ldots. \tag{5}$$

The resonance wavelength and the anti-resonance wavelength are obtained to be $\lambda_{\rm r} = 2d\sqrt{n_2^2 - n_1^2}/(m + 1/2)$ and $\lambda_{\rm ar} = 2d\sqrt{n_2^2 - n_1^2}/m$, where d is the cylinder diameter, n_1 and n_2 are the effective indices of silica structure and high index cylinders, $m = 1, 2, \ldots$. For the fundamental mode and higher-order modes, $\lambda_{\rm r}$ and $\lambda_{\rm ar}$ correspond to the narrower transmission dip and the broader high transmission window respectively. Thus, the resonance and the anti-resonance characteristics are well predicted,

5. Conclusions

The filled material index and the cladding structure parameters have important influences on the characteristics of band-gap and mode in ARGPCF. Based on the designed ARGPCF operating at the near-infrared wavelength, the influences of high index cylinders, glass interstitial apexes and silica structure are also analysed. By the equivalent planar waveguide theory, the resonance and anti-resonance characteristics can be well analysed.

References

[1] Yan P M and Shum P 2005 *IEEE Photonics Technol. Lett.* **30** 465

[2] Ho K M, Chan C T and Soukoulis C M 1990 *Phys. Rev. Lett.* **65** 3125

[3] Yuan J H, Hou L T, Zhou G Y, Wei D B, Chen C, Wang Q Y, Hu M L and Liu B W 2008 *Chin. Phys. Lett.* **25** 1541

[4] Mi Y, Hou L T, Zhou G Y, Wang K, Chen C, Gao F, Liu B W and Hu M L 2008 *Acta Phys. Sin.* **57** 3583 (in Chinese)

[5] Yuan J H, Hou L T, Zhou G Y, Wei D B, Wang H Y, Dong S R, Wang Q Y, Liu B W and Hu M L 2008 *Acta Phys. Sin.* **57** 4230 (in Chinese)

[6] Meng J, Hou L T, Zhou G Y, Gao F, Yuan J H and Wei D B 2008 *Chin. Phys.* B **17** 3779

[7] Yuan J H, Yu C X, Sang X Z, Li W J, Zhou G Y, Li S G and Hou L T 2009 *Chin. Phys. Lett.* **26** 034211-1

[8] Yuan J H, Yu C X, Sang X Z, Zhou G Y, Li S G and Hou L T 2009 *Appl. Phys.* B **96** 337

[9] Yariv Y A and Marom E 1978 *J. Opt. Soc. Am.* B **68** 1196

[10] Cerqueira S Jr, Luan F, Cordeiro C M B, George A K and Knight J C 2006 *Opt. Express* **14** 926

[11] Roberts P J, Williams D P, Mangan B J, Sabert H, Couny F, Wadsworth W J, Birks T A, Knight J C and Russell P S J 2005 *Opt Express* **13** 8277

[12] Yu X, Shum P, Yan M and Ren G B 2008 *IEEE Photonics Technol. Lett.* **20** 1141

[13] Fuerbach A, Steinvurzel P, Dolger J A and Eggleton B J 2005 *Opt. Express* **13** 2977

[14] Litchinitser N M, Dunn S C, Usner B, Eggleton B J, White T P, McPhedran R C and Martijin de Sterke C 2003 *Opt. Express* **11** 1243

[15] Birks T A, Pearce G J and Bird D M 2003 *Opt. Express* **14** 9483

[16] Couny F, Benabid F, Roberts P J, Burnett M T and Maier S A 2007 *Opt. Express* **15** 325

[17] Guo S P and Albin S 2003 *Opt. Express* **11** 167

[18] Ferrando A, Silvestre E, Miret J J, Andres P and Andres M V 1999 *Opt. Lett.* **24** 276

[19] Canning J, Buckley E, Lyytikainen K and Ryan T 2003 *Opt. Commun.* **205** 95

[20] Smith C M, Venkataraman N, Gallagher M T, Müller D, West J A, Borrelli N F, Allan D C and Koch K W 2003 *Nature* **424** 657

[21] Amezcua-Correa R, Broderick N G R, Petrovich M N, Poletti F and Richardson D J 2006 *Opt. Express* **14** 7974

[22] Steinvurzel P, Martijn de Sterke C, Steel M J, Kuhlmey B T and Eggleton B J 2006 *Opt. Express* **14** 8797

[23] Sun J, Chan C C, Shum P and Poh C L 2008 *Opt. Lett.* **33** 809

[24] Ren G B, Shum P, Hu J J, Yu X and Gong Y D 2008 *IEEE Photonics Technol. Lett.* **20** 602

[25] Du J B, Liu Y G, Wang Z, Zou B, Liu B and Dong X Y 2008 *Appl. Opt.* **447** 5321